Self-organisation of robot assemblies

Author: Andreu Gironella Martínez, agironma8@alumnes.ub.edu
Facultat de Física, Universitat de Barcelona, Diagonal 645, 08028 Barcelona, Spain.

Advisor: Demian Levis, levis@ub.edu and Co-Advisor: Juan Pablo Carrillo-Mora, jpcarrillo-mora@ub.edu

Abstract: Hexbug robots are self-propelled particles that can behave as both chiral and non-chiral active Brownian particles. We experimentally determined key parameters: self-propulsion speed, chirality, rotational diffusion and self-alignment length, for seven robots by studying their free trajectories and angular dynamics under translational forcing. To explore collective behavior, we assembled active trimers by linking three robots in a linear chain with rods allowing free rotation. From these experiments, we developed a trimer model and ran extensive numerical simulations to analyze its dynamics. Our results reveal two dynamical regimes depending on the central robot's chirality: one resembling active Brownian motion and another similar to chiral run-and-tumble dynamics. This behavior emerges from the interplay of two time scales related to chirality and self-alignment. By analyzing center-of-mass trajectories, we studied the mean squared displacement to measure the effective translational diffusion coefficient of the trimer. It decreases with chirality in the first regime but increases in the second, where tumbling events emerge. A minimum occurs where the two time scales balance, indicating a smooth crossover.
Keywords: active particles, chirality, self-organization, active transport, self-propelled robots.
SDGs: 9. Industry, innovation and infrastructure and 14. Life below water.

I. INTRODUCTION

Active matter are non equilibrium soft-condensed matter systems composed by self-driven units which are able to convert energy from their environment into directed motion [1]. This active motion can be found in a wide range of systems at different length scales [2]. The self-propelled agents that compose these systems are called *active particles* and can be of biological or artificial origin [2]. Biological active particles include various types of entities, ranging from microscopic swimmers such as cells and bacteria to macroscopic organisms, including fish and birds, which exhibit collective motion in schools or flocks [1, 3]. Meanwhile, some examples of artificial active particles are *Janus particles* on the micro scale and Hexbugs self-propelled robots on the centimeter scale [3, 4].

In systems where interactions between active units do not influence their orientations and are limited to standard repulsive and attractive forces, the system is classified as *scalar* active matter. In contrast, most active matter systems exhibit orientational degrees of freedom, enabling additional interaction mechanisms. A widely adopted approach to introduce interactions involving polarity in such systems, is the possibility of couplings between orientations and translations [4]. In particular, the self-aligning torque is a type of interaction that couples the translation of a polar particle with its own orientation [4].

Among the active particles we find different types of dynamics that differ, for example, in the way they change direction in time. In this report, we focus on *Active Brownian Particles* (ABPs) and *Run-and-Tumble Particles* (RTPs). In both cases, the particles self-propel at a fixed speed v_0 along a body-axis $\hat{\mathbf{n}}$, which reorients either through gradual angular diffusion in the case of ABPs, or through sudden and complete randomization in the case of RTPs [5].

Beyond translational behavior, active particles may also exhibit *chiral motion*, where their trajectories follow circular paths as a result of persistent rotational motion. This phenomenon arises from an internal or effective torque that the particle intrinsically possesses, leading to a breaking of the left-right symmetry in its orientation dynamics [6]. *Chirality* then, refers to the property of a trajectory of being non-superimposable with its mirror image [6]. This leads to a directional bias such as a preferred sense of rotation which makes trajectories spin in smaller or larger circles depending on the particle chirality value.

A key quantity to characterize the transport of active particles is the *effective translational diffusion coefficient*, which quantifies how rapidly a particle spreads in space over time [3]. Unlike passive systems, where diffusion arises only from thermal noise, in active systems this coefficient reflects the combined effect of self-propulsion, reorientation mechanisms, and interactions [7]. This coefficient serves as a measure of *active transport* by capturing how efficiently a particle converts internal energy into spatial exploration, an efficiency we will refer to as *effective transport* throughout this thesis.

In this memoir, we specifically analyze the motion and transport of toy robots (Hexbugs) that, when considered individually, behave as a *self-aligning active Brownian particle* (SA-ABP), and when configured as a trimer, exhibit different behaviors, including *chiral run-and-tumble particle* (cRTP). To achieve this, we conducted laboratory experiments to characterize the individual behavior of the Hexbugs through free trajectories and a dedicated self-alignment experiment [8]. This allowed us to later

investigate their collective behavior in a simple structure such as a trimer, primarily through long numerical simulations. In these simulations, we observed that the effective translational diffusion coefficient of the trimer exhibits opposite trends in two clearly defined regimes, depending on whether it behaves like a chiral ABP or a chiral RTP.

This unexpected behavior motivated a closer examination of how collective dynamics influence transport. While individual robots show reduced diffusion with increasing chirality, the trimer displays a non-monotonic trend: diffusion first decreases with chirality, then rises again when frequent reorientations enhance motion. This suggests that linking a highly chiral robot into a trimer can improve its spatial exploration, driven by a transition from smooth circular paths to more erratic, run-and-tumble-like dynamics.

II. MODELING A HEXBUG AS AN ACTIVE PARTICLE

Hexbugs are robots that achieve self-propulsion through vibration, which leads to persistent random motion patterns [9]. We demonstrate that this motion can be described as chiral SA-ABP. Then, to model their dynamics, we consider that the particles move with a constant self-propulsion speed v_0 in the direction of its director vector $\hat{\mathbf{n}}$ [10].

FIG. 1: Images of a Hexbug toy-robot and a trimer used in the experiments.

The motion of each particle is governed by the following set of coupled overdamped stochastic differential equations [11, 12]:

$$\dot{\mathbf{r}}_i = v_0\,\hat{\mathbf{n}}_i - \mu \sum_{j\neq i} \nabla_i U_{ij} \tag{1}$$

$$\dot{\theta}_i = \omega_0 + \frac{1}{l_a}|\dot{\mathbf{r}}_i|\sin(\phi_i - \theta_i) + \sqrt{2D_r}\,\eta_i \tag{2}$$

In Eq. (1) the position corresponds to the 2D vector $\mathbf{r}_i = [x_i(t), y_i(t)]$, v_o is the self-propulsion speed, $\hat{\mathbf{n}}_i = (\cos\theta_i, \sin\theta_i)$ is the director vector, μ is the mobility of the particle and $-\nabla_i U_{ij}$ is the force exerted by particle j on particle i. In equation (2) the variation of the particle orientation θ_i depends on three terms: the intrinsic chirality ω_0, the self-alignment (that depends on a self-alignment length l_a), which measures how quickly the particle orientation aligns with its direction of motion denoted by the angle ϕ_i. And finally, rotational diffusion, including a rotation diffusion coefficient D_r and zero mean white noise with unit variance η_i. Since we are working with macroscopic particles, translational diffusion term is not needed in contrast with microscale systems [9].

III. INDIVIDUAL HEXBUG PARAMETERS STUDY

In order to perform the calculations and simulations for our trimers, we need to know the individual motility parameters for each of the robots that we will use in our experiments. For individual particle free trajectories, Hexbugs don't feel any force exerted between particles. Then $-\nabla_i U_{ij}$ will be zero and the orientation of the robot will be aligned with the orientation of its movement $\phi = \theta$. Therefore, Eqs. (1) and (2) reduce to:

$$\dot{\mathbf{r}} = v_0\hat{\mathbf{n}}, \qquad \dot{\theta} = \omega_0 + \sqrt{2D_R}\,\eta_i \tag{3}$$

In our experiments we characterized the motility parameters of seven different Hexbugs robots by tracking their free trajectories individually and also by forcing their translation in a straight channel. These two experiments are sufficient to obtain the self-propulsion speed, chirality, rotational diffusion coefficient and self-alignment length of each robot.

In the lab, we used a squared 120×120 cm^2 light table for our robots to move freely. A GoPro Hero 5 camera is mounted on the table to record the experiments from a zenithal view. This is what allows us to approximate the system in 2D. To model the Hexbugs as circular particles and facilitate their assembly in later experiments, we used circular structures 3D-printed to hold each robot securely. These structures feature a vertical rod at their center, which is necessary to connect the Hexbugs together. The diameter of each structure is $D_{\text{Hexbug}} = 5.7\,\text{cm}$.

From the tracked positions and orientations of particles in experimental free trajectories, the self-propulsion velocity and the particle chirality can be estimated as:

$$v_0 = \left\langle \frac{\Delta r}{\Delta t} \right\rangle, \qquad \omega_0 = \left\langle \frac{\Delta\theta}{\Delta t} \right\rangle \tag{4}$$

where Δr is the distance traveled by the robot during the time interval Δt, and $\Delta\theta$ represents the change in the orientation angle θ_i of the robot over that same Δt.

Hence, the rotational diffusion coefficient is:

$$D_R = \left\langle \frac{(\Delta\theta - \omega_0\Delta t)^2}{2\Delta t} \right\rangle \tag{5}$$

Details on video data acquisition and tracking method are available in the Supplementary Material Sec. VI B.

On the other hand, to obtain the self-alignment length, we put the Hexbug on a straight channel which made

it move only through $x-$axis but keeping free angular movement. The robot was tethered to a string pulled by a motorized system, allowing us to set different pulling speeds and ensure consistent force application. This allowed us to change the velocity at which the robot moved and measure how long it takes for the robot to align its orientation with its displacement (i.e. $\phi \simeq \theta$).

In these measurements, $\omega_0 \ll v/l_a$ since the robot only moves in a straight line $\dot{r} = v$, D_r is set to zero to obtain a deterministic solution, and $\phi_i = 0$ because the imposed velocity points along the x-axis, which is also the reference direction for measuring the angle. Therefore, we can rewrite Eq. (2) as $\dot{\theta} = -\frac{1}{\tau_{sa}} \sin(\phi - \theta)$, where $\tau_{sa} = \frac{l_a}{v}$. Solving this differential equation, we obtain:

$$\theta(t) = 2 \arctan\left[\tan\left(\frac{\theta_0}{2}\right) e^{-t/\tau_{sa}}\right] \tag{6}$$

IV. FREE TRAJECTORIES AND SELF-ALIGNMENT RESULTS

To study free trajectories, we filmed multiple individual runs for each robot on the light table until they reached the wall. More chiral Hexbugs produce longer trajectories due to their tendency to rotate in place, whereas low-chirality ones follow shorter, noisier, and more linear paths because of rotational diffusion. For the self-alignment experiment (see Fig. 2) we got an assembly that allowed us to fix different velocities of the string that pulls the Hexbug, so we recorded a set of videos for each robot at different string forces [8].

Videos were processed with FIJI [13] to enable precise tracking of position (x, y) and orientation θ (see Supplementary Material, Sec. VI B). Using the tracking data from the free trajectory experiments, we apply equations (4) and (5) to extract the parameters: v_0, ω_0, and D_r. Then, to determine l_a, we fit the self-alignment experiment data using Eq. (6). All individual Hexbug parameters obtained through these procedures are summarized in Supplementary Material Table I.

V. HEXBUG TRIMERS AS PARTICLES

Knowing the motility parameters of Hexbugs and how they behave individually, it is interesting to study how they behave as a *Hexbug trimer*, a unit of 3 of them (see Fig. 1). To do that, we perform various lab experiments and complement them with large numerical simulations with standardized parameters for our robots.

In order to study the dynamics of the trimer's center-of-mass, by tracking the position $\boldsymbol{r}_i(t)$ of each robot, we can obtain the position of the center-of-mass by averaging the position of the robots. Therefore, $\vec{r}_{\rm CM} = (x_{\rm CM}, y_{\rm CM})$ can be expressed as: $\vec{r}_{\rm CM}(t) = \frac{1}{N}\sum_{i=1}^{N} \vec{r}_i(t)$. Then, mean squared displacement (MSD) of the center-of-mass position is calculated as follows:

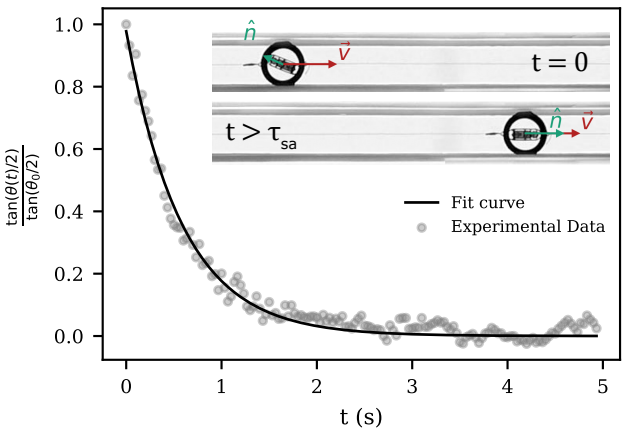

FIG. 2: Self-alignment experiment for Robot 1. The experimental angular relaxation dynamics under translational forcing is fitted using Eq. (6). The two inset frames show experimental snapshots corresponding to the initial and final states used to compute the fitted curve, which corresponds to $\tau_{sa} = 0.584$ s.

$$\mathrm{MSD}_{\rm CM}(t) = \left\langle \left|\vec{r}_{\rm CM}(t_0 + t) - \vec{r}_{\rm CM}(t_0)\right|^2 \right\rangle_{t_0} \tag{7}$$

where $\langle\cdot\rangle_{t_0}$ denotes the time average over all initial times t_0, t is a lag time, and the squared modulus corresponds to the squared distance traveled by the center of mass between t_0 and $t_0 + t$. This MSD is very useful to study the type transport of the Hexbug trimer.

Recalling the equations from our initial model (1) and (2), the trimers exhibit two competing timescales that give rise to different behaviors in the system. The first is the characteristic alignment timescale τ_a, and the second is the characteristic chirality timescale τ_c.

$$\tau_a = \frac{l_a}{v_0}\,, \quad \tau_c = \frac{1}{2|\omega_0|} \tag{8}$$

Depending on which of these two timescales dominates in the central robot of the trimer, a range of distinct behaviors emerges. These are explored through simulations and experiments throughout this thesis.

It is also interesting to examine the effective translational diffusion coefficient, $D_{\rm eff}$, in our trimers. The dominance of the characteristic self-alignment time can lead to a significant change in the behavior of the particles, which may cause variations in effective transport in a different manner compared to individual robots. To compute $D_{\rm eff}$, for sufficiently long times in 2D, the center-of-mass MSD grows linearly [7]: $\mathrm{MSD}_{\rm CM}(t) \approx 4D_{\rm eff}\, t$.

On a log-log scale, the slope $m = \frac{d\log(\mathrm{MSD}(t))}{d\log(t)}$ corresponds to the diffusion exponent α in $\mathrm{MSD}(t) \sim t^{\alpha}$. Active particles show a ballistic regime ($\alpha \approx 2$) at short times and a diffusive regime ($\alpha \approx 1$) at long times, where

$$D_{\rm eff} = \frac{1}{4}\frac{d}{dt}\mathrm{MSD}(t) \tag{9}$$

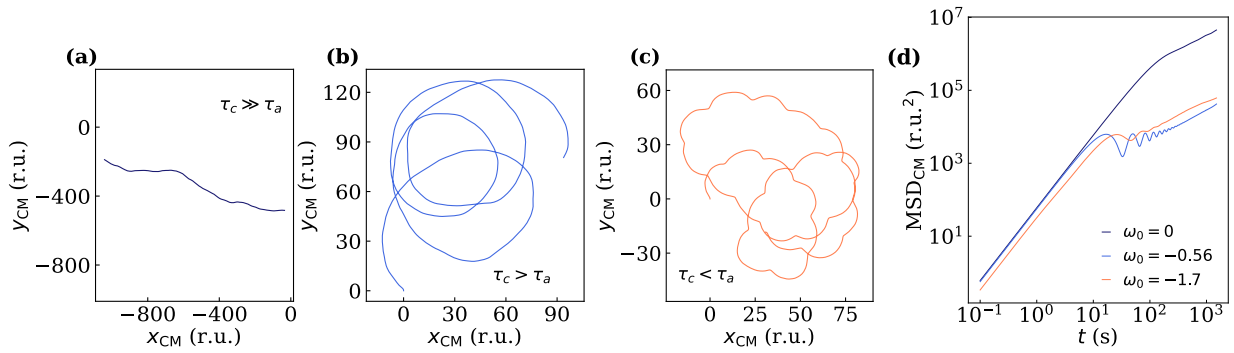

FIG. 3: Trajectories of the trimer's center-of-mass in simulations for three different values of the central robot's chirality: (a) $\omega_0 = 0$ s^{-1}, (b) $\omega_0 = -0.56$ s^{-1}, and (c) $\omega_0 = -1.7$ s^{-1}. All lateral robots remain non-chiral. (d) Log-log plot of the mean squared displacement (MSD) of the center-of-mass corresponding to the three cases. For all the trajectories $\tau_a = 0.885$ s.

A. Exploratory experimental results

For our trimer experiments, we used the same seven Hexbugs and light table as in the free trajectories, connecting them with two rigid sticks that allowed rotational freedom. Most combinations formed a stable triangular packing that moved along circular paths. However, when placing the most chiral robot (Robot 7) in the center, the trimer exhibited periodic folding and unfolding, revealing a distinct collective behavior. The contrast between these two regimes suggests that when $\tau_c < \tau_a$ (see Eq. (8)), the trimer stops behaving like a self-aligned active Brownian particle (SA-ABP) and instead begins to exhibit run-and-tumble particle (RTP) characteristics. This transition is associated with the periodic folding and unfolding of the chain, causing abrupt changes in the center-of-mass trajectory.

Experimentally, to demonstrate that these trimers can move approximately as chiral RTPs, we placed robot 7 in the middle position of the trimer and selected Hexbugs 3 and 6 as the outer robots due to their very low chirality. We tracked a trimer trajectory for 35 minutes and obtained an experimental value for its effective diffusion coefficient, $D_{\text{eff}} = 3.042\,\text{cm}^2/\text{s}$. This value is shown in Fig. 4 in reduced units (r.u.) alongside our simulation results for comparison. Since our video was not long enough to fully reach the MSD diffusive regime , D_{eff} is calculated with Eq. (10) from Supplementary Material.

B. Simulations results

The model used in the simulations is the one described in Eqs. (1) and (2) for each Hexbug. The main approximation used is to assume that the robots are connected by springs with a very high elastic constant k, such that they can be approximated as rigid, like the sticks we used to connect the robots in our lab. Taking this into account, the forces experienced by each robot are $\mathbf{F}_{ij} = -\nabla_i U_{ij} = k\,(\|\mathbf{r}_{ij}\| - 2r_p)\,\hat{\mathbf{r}}_{ij}$, where $\|\mathbf{r}_{ij}\|$ is the distance between robot i and robot j, r_p the Hexbug radius and $\hat{\mathbf{r}}_{ij}$ is the unit vector in the direction of $\mathbf{r}_{ij}$.

The other robots parameters are standardized using an average v_o, D_r and l_a of some of the robots used in our experiments. They are expressed in non-dimensional units. Length is scaled by the particle radius $r_p = 1$. The means used are $\bar{v}_0 = 7.87$ r.u., $\bar{D}_r = 0.02$ s^{-1} and $\bar{l}_a = 6.96$ r.u. For the chirality, the Hexbugs positioned at the ends of the chain are assigned zero values, while the chirality of the central robot is varied across six values ranging from 0 to -2.26 s^{-1} (see Supplementary Table II).

Therefore, all simulations share the same $\tau_a = 0.885\,\text{s}$, while τ_c varies to modify the central robot's chirality. To study the effect of this variation, we plotted the center-of-mass trajectories and calculated their translational MSD. Figure 3 shows three qualitatively distinct behaviors depending on the central chirality. Panel (a) resembles non-chiral active Brownian motion, panel (b) displays typical circular motion of a chiral ABP, and panel (c) exhibits periodic tumbling events characteristic of a chiral Run-and-Tumble particle. For all trajectories, the MSD shown in panel (d) initially grows ballistically with a slope of 2 in the log-log scale, indicating a quadratic time dependence, before crossing over to a diffusive regime with slope 1, corresponding to linear growth in time. The effective diffusion coefficient D_{eff} is extracted from this linear regime using Eq. (9). In the non-chiral case ($\omega_0 = 0\,\text{s}^{-1}$), the ballistic-to-diffusive transition occurs smoothly at longer times, consistent with persistent motion. As chirality increases ($\omega_0 = -0.56\,\text{s}^{-1}$), the trimer follows confined circular orbits, leading to the lowest long-time MSD values. At stronger chirality ($\omega_0 = -1.7$ s^{-1}), periodic tumbling events allow the system to escape this confinement, increasing the MSD again. In both chiral cases, the transition to diffusion happens earlier, reflecting a loss of directional persistence due to rotational dynamics.

Notably, despite its stronger chirality, the highest chirality case exhibits a slightly larger D_{eff} than the intermediate one (Fig. 4), due to reorientation events resembling tumbles that enhance spatial exploration. These results highlight how tuning ω_0 controls the balance between chiral and aligning timescales (τ_c and τ_a), giving

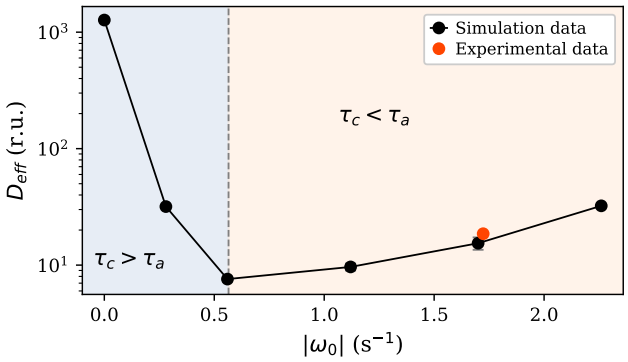

FIG. 4: Effective diffusion coefficient D_{eff} as a function of the absolute value of the central chirality $|\omega_0|$. The y-axis is shown in logarithmic scale, while the x-axis remains linear. Black markers represent values obtained from numerical simulations, while the orange marker corresponds to the experimentally measured D_{eff} for the robot chain 3–7–6 (connected in that order). The vertical dashed line indicates the point where the chiral time τ_c equals the alignment time τ_a, separating two distinct dynamical regimes of the trimer.

rise to distinct dynamical regimes and a non-monotonic transport efficiency.

VI. CONCLUSIONS

For the Hexbugs studied, we have observed in our lab experiments while measuring their parameters, that they behave as SA-ABP particles (either chiral or not) when following individual trajectories (as seen in Suplementary Material Fig. 5). This allows us to qualitatively see how effective transport decreases as the chirality of the particle increases.

When connecting three robots to form a trimer where the joints between them allow free rotation, we found that the central robot's chirality introduces a competition between the characteristic chiral time scale τ_c and the alignment time scale τ_a. Analyzing the trajectories of the center of mass, we identified three regimes: for $\tau_c \gg \tau_a$, the trimer behaves like an ABP; for $\tau_c > \tau_a$, it resembles a chiral ABP; and for $\tau_c < \tau_a$, the motion resembles to a chiral run-and-tumble particle (cRTP). The different regimes are also evident in the corresponding MSD curves, where increased chirality leads to the appearance of oscillations and a faster transition to the diffusive regime.

In contrast with the monotonic dependence of D_{eff} on chirality in isolated robots, the trimer shows a non-monotonic behavior: D_{eff} reaches a minimum when $\tau_c \simeq \tau_a$, corresponding to the most confined, chiral motion. Beyond this point, as τ_c decreases further and tumbles become more frequent, we observe an enhancement in effective transport, even though the central robot is more chiral. These results suggest that connecting a highly chiral robot to form a trimer can significantly enhance its effective diffusion, allowing it to explore larger areas in less time. This enhancement is directly linked to changes in the system's collective dynamics, which transition between ABP-like and RTP-like behavior depends on the balance between τ_c and τ_a.

Acknowledgments

I would like to thank Demian Levis, my thesis advisor, for giving me the opportunity to carry out this work within his research group. I am especially grateful to Juan Pablo Carrillo-Mora for his ongoing support and guidance, and for working alongside me throughout all the experiments.

[1] M. C. Marchetti *et al.*, *Hydrodynamics of soft active matter*, Rev. Mod. Phys. **85**, 1143–1189 (2013).
[2] F. Schweitzer, *Active Particles*, in *Brownian Agents and Active Particles*, Springer Series in Synergetics (Springer, Berlin, Heidelberg), Chapter 2 (2007).
[3] C. Bechinger *et al.*, *Active particles in complex and crowded environments*, Rev. Mod. Phys. **88**, 045006 (2016).
[4] P. Baconnier *et al.*, *Self-Aligning Polar Active Matter*, arXiv:2403.10151 (2024).
[5] A. P. Solon, M. E. Cates, and J. Tailleur, *Active Brownian Particles and Run-and-Tumble Particles: a Comparative Study*, arXiv:1504.07391 (2015).
[6] B. Liebchen and D. Levis, *Chiral Active Matter*, EPL **139**, 67001 (2022).
[7] P. Romanczuk *et al.*, *Active Brownian particles*, Eur. Phys. J. Spec. Top. **202**, 1 (2012).
[8] J. P. Carrillo-Mora, A. Garcés, and D. Levis, *Depinning and activated motion of chiral self-propelled robots*, arXiv:2506.20610 (2025).
[9] A. Barona Balda *et al.*, *Playing with Active Matter*, Am. J. Phys. **92**, 847–858 (2024).
[10] A. Callegari and G. Volpe, *Numerical Simulations of Active Brownian Particles*, in *Active Matter*, edited by G. Volpe, Springer Series in Bio- and Neurosystems, Springer (2022), pp. 189–218.
[11] R. Großmann, L. Schimansky-Geier, and P. Romanczuk, *Active Brownian particles with velocity-alignment and active fluctuations*, New J. Phys. **14**, 073033 (2012).
[12] P. Baconnier *et al.*, *Selective and collective actuation in active solids*, Nat. Phys. **18**, 1238–1244 (2022).
[13] J. Schindelin *et al.*, *Fiji: an open-source platform for biological-image analysis*, Nat. Methods **9**, 676–682 (2012).

Autoorganització d'assemblatges de robots

Author: Andreu Gironella Martínez, agironma8@alumnes.ub.edu
Facultat de Física, Universitat de Barcelona, Diagonal 645, 08028 Barcelona, Spain.

Advisor: Demian Levis, levis@ub.edu and Co-Advisor: Juan Pablo Carrillo-Mora, jpcarrillo-mora@ub.edu

Resum: Els robots Hexbug són partícules autopropulsades que poden comportar-se tant com a partícules actives brownianes quirals, com no quirals. Vam determinar experimentalment paràmetres clau com la velocitat d'autopropulsió, la quiralitat, la difusió rotacional i la longitud d'autoalineament, per a set robots estudiant les seves trajectòries lliures i la dinàmica angular sota forçament translacional. Per a poder explorar el comportament col·lectiu, vam ajuntar els robots en trímers actius enllaçant tres robots en una cadena lineal amb barres que permeten la rotació lliure. A partir d'aquests experiments, vam desenvolupar un model per als trímers i vam realitzar simulacions numèriques per analitzar la seva dinàmica. Els nostres resultats revelen dos règims dinàmics depenent de la quiralitat del robot central: un que correspon al moviment brownià actiu i un altre similar a la dinàmica de run-and-tumble quiral. Aquest comportament sorgeix de la interacció de dues escales temporals vinculades a la quiralitat i a l'autoalineament. Analitzant les trajectòries del centre de massa, hem estudiat el desplaçament quadràtic mitjà per extreure el coeficient efectiu de difusió translacional. Aquest disminueix amb la quiralitat en el primer règim, però augmenta amb la quiralitat en el segon, a causa dels tombs que generen el moviment de run-and-tumble. Observem un valor mínim on les dues escales temporals s'equilibren, indicant el punt on canvien els règims.
Paraules clau: partícules actives, quiralitat, transport actiu, autoorganització, robots autopropulsats
ODSs: 9. Indústria, innovació, infraestructures i 14. Vida submarina

Objectius de Desenvolupament Sostenible (ODSs o SDGs)

1. Fi de la es desigualtats		10. Reducció de les desigualtats	
2. Fam zero		11. Ciutats i comunitats sostenibles	
3. Salut i benestar		12. Consum i producció responsables	
4. Educació de qualitat		13. Acció climàtica	
5. Igualtat de gènere		14. Vida submarina	X
6. Aigua neta i sanejament		15. Vida terrestre	
7. Energia neta i sostenible		16. Pau, justícia i institucions sòlides	
8. Treball digne i creixement econòmic		17. Aliança pels objectius	
9. Indústria, innovació, infraestructures	X		

L'estudi dels Hexbug com a sistemes actius i autònoms ofereix una contribució significativa en l'àmbit de la indústria, la innovació i les infraestructures (ODS 9), en particular en el compliment de l'objectiu 9.5, que busca millorar la investigació científica i augmentar la capacitat tecnològica per fomentar la innovació. El desenvolupament i l'anàlisi del comportament dinàmic dels Hexbug poden impulsar avenços tecnològics en la creació de dispositius robòtics innovadors amb aplicacions en diversos sectors. Aquesta recerca afavoreix el disseny d'infraestructures intel·ligents i sostenibles que responen a les necessitats actuals de modernització i eficiència. A més, la comprensió dels moviments autònoms d'aquests sistemes té un interès directe per a la conservació de la vida submarina (ODS 14), especialment en relació amb l'objectiu 14.2, que promou la gestió i protecció dels ecosistemes marins i costaners. Això pot facilitar el desenvolupament de microrobots destinats a l'exploració, el monitoratge i la protecció dels ecosistemes marins, contribuint així a la gestió sostenible dels recursos oceànics.

SUPPLEMENTARY MATERIAL

A. Free trajectories experiments

In our free trajectory experiments we tracked seven different robots and that allowed us to represent some of their free trajectories (Fig. 5.). When compared to their parameters exposed in Table I, we can qualitatively see how the more chiral the robots are, the longer trajectory we can represent, as their effective transport becomes lower and so does the D_{eff}. This basically means, it takes longer for them to hit the walls of our light table. Therefore, their exploration area is very confined.

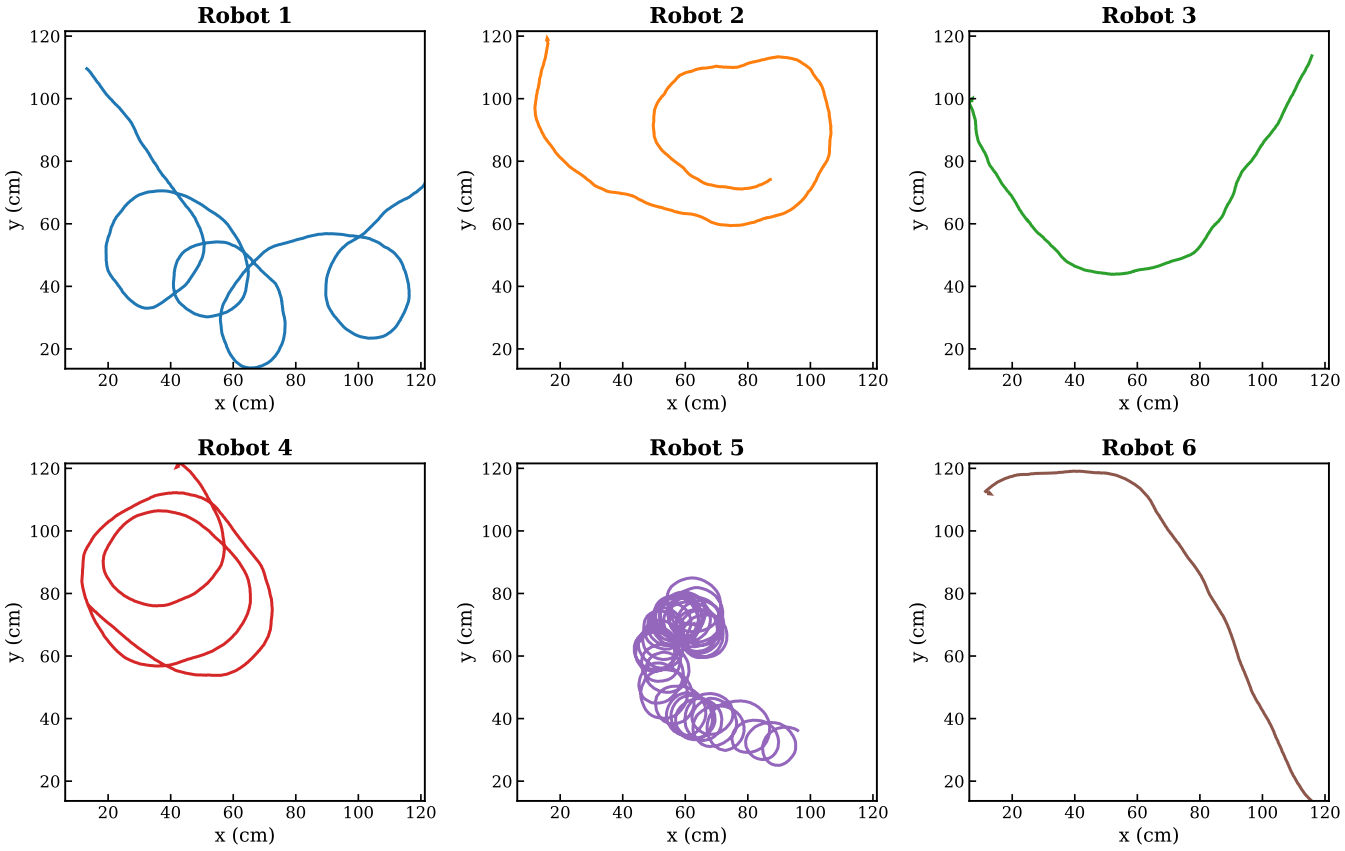

FIG. 5: Experimental free trajectories for 6 of our robots

TABLE I: Experimental values for each robot of self-propel velocity v_o, chirality ω_o, rotational diffusion coefficient D_R and self-alignment distance l_a with their standard error.

Robot	v_0 (cm/s)	ω_0 (rad/s)	D_R (s^{-1})	l_a (cm)
Robot 1	8.40 ± 0.02	0.323 ± 0.010	0.0144 ± 0.0004	8.9 ± 0.5
Robot 2	6.25 ± 0.02	0.103 ± 0.012	0.0165 ± 0.0005	7.8 ± 0.5
Robot 3	7.49 ± 0.02	-0.057 ± 0.010	0.0145 ± 0.0004	7.8 ± 0.4
Robot 4	9.74 ± 0.02	-0.147 ± 0.012	0.0107 ± 0.0003	6.5 ± 0.4
Robot 5	7.85 ± 0.01	-1.070 ± 0.008	0.0111 ± 0.0002	5.9 ± 0.3
Robot 6	8.35 ± 0.01	0.012 ± 0.018	0.0419 ± 0.0181	13.9 ± 0.9
Robot 7	9.53 ± 0.02	-1.723 ± 0.012	0.0490 ± 0.0003	8.5 ± 0.5

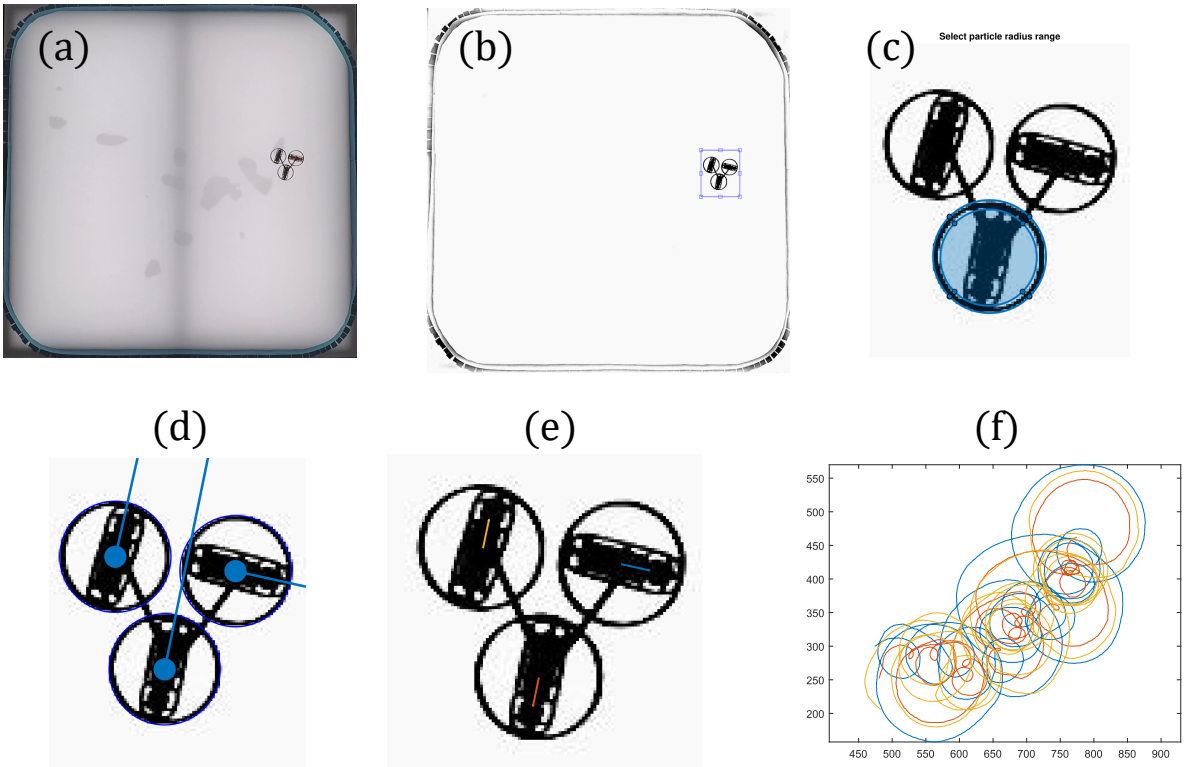

FIG. 6: Sequence of images illustrating the video processing and tracking positioning for the Hexbug robots. (a) A raw frame from the experimental video showing three trimers. (b) The same frame after background subtraction and conversion to binary format. (c) Detection of the particle's inner and outer circular boundaries. (d) Identification of the robot centers; however, some orientations are initially inverted, pointing toward the tail. (e) Correction of orientation vectors to ensure they point toward the head, distinguished by its more rounded shape. (f) Tracked trajectories of the three robots over time, used to verify the accuracy and consistency of the extracted data.

B. Tracking and video processing

To analyze our experimental videos, we first needed to preprocess them. This involved converting the videos to black and white, subtracting the background noise or blemishes, and adjusting the contrast until we obtained a completely white background with one or more robots appearing in solid black and with good definition. This preprocessing was carried out using FIJI [13].

To track the position of each particle in the recorded videos, we apply a standard circle detection algorithm to each frame. The center of the detected circle is identified as the position of the particle at that time frame. For orientation tracking, we define a mask around the previously detected circular region and fit an ellipse to the main body of the robot within this region. The orientation of the particle is then extracted from the angle of the major axis of the fitted ellipse, which serves as an estimate of the robot's orientation in the plane.

In our case, we measure the position (x, y) for each frame of the video through video tracking of the free trajectories for each robot. Δr and $\Delta\theta$ of Eq. (4) is obtained by substracting consecutive positions for a $\Delta t = 1/30$ since we recorded in 30 fps.

C. Effective diffusion coefficient

When the diffusive regime is not fully reached, D_{eff} can be computed from the velocity autocorrelation using the generalized Green-Kubo relation:

$$D_{\text{eff}} = \int_0^\infty \langle \mathbf{v}(t_0) \cdot \mathbf{v}(t_0 + t) \rangle_{t_0} \, dt \tag{10}$$

TABLE II: Effective diffusion coefficients D_{eff} for trimers with varying central chirality ω_0. Each row shows three independent measurements, along with the mean and its standard deviation. The persistence time τ_c is also reported for each case. For all these trimers $\tau_a = 0.885$ s

ω_0 (s^{-1})	τ_c (s)	$D_{\text{eff}}^{(1)}$ (r.u.)	$D_{\text{eff}}^{(2)}$ (r.u.)	$D_{\text{eff}}^{(3)}$ (r.u.)	$\langle D_{\text{eff}} \rangle \pm \sigma$ (r.u.)
-2.26	0.221	33.66	31.90	31.30	32.28 ± 1.00
-1.70	0.294	16.74	12.75	16.76	15.42 ± 1.88
-1.12	0.446	9.74	10.42	8.78	9.65 ± 0.67
-0.56	0.893	7.94	7.66	7.15	7.59 ± 0.33
-0.28	1.786	31.43	31.18	32.83	31.81 ± 0.72
0	∞	1269.65	1284.56	1258.31	1270.84 ± 10.75